New Charge-Transfer Complexes of Organochalcogenide Compound Based on Aryl Acetamide Group with Quinones: Synthesis, Characterization, Antioxidant, and Computational Study

Attared Fadhel Hassan[1], Nahed Hazim Al-Haidery[1], Suhad Rajab Kareem[1], Sabah Abbas Malik[2], Shaker Abdel Salem Al-Jadaan[3], and Nuha Hussain Al-Saadawy[4*]

[1]*Department of Chemistry, College of Science, University of Basrah, Basrah 61004, Iraq*

[2]*Department of Pharmaceutical Chemistry, Branch of Pharmaceutical Chemistry, University of Kufa, Najaf 54001, Iraq*

[3]*Department of Pharmaceutical Chemistry, College of Pharmacy, University of Basrah, Basrah 61004, Iraq*

[4]*Department of Chemistry, College of Science, University of Thi-Qar, Muthanna 64001, Iraq*

Corresponding author:

email: nuhaalshather@yahoo.com

Received: August 29, 2023
Accepted: October 21, 2023

DOI: 10.22146/ijc.88463

Abstract: *This study aims to prepare charge transfer complexes derived from organochalcogenide of arylamide derivatives with different quinones. A new charge-transfer complexes have been developed through a direct reaction between $(PhNHCOCH_2)_2Se$, $(o\text{-}CH_3PhNHCOCH_2)_2Se$, and $(PhCH_2NHCOCH_2)_2E$, where E = S, Se, and Te are electron donors and different quinones are electron acceptors. The quinones used in the reaction were 2,3-dichloro-5,6-dicyanobenzoquinones (DDQ), 7,7',8,8'-tetracyanoquinodimethane, and tetracyanoethane. The electron donors and electron acceptor mol were 1:1, and the reaction was conducted in acetonitrile. Infrared, ^1H and ^{13}C-NMR spectroscopic data characterized all complexes. The complexes' antioxidant activity was evaluated through α,α-diphenyl-β-picrylhydrazyl at 10–0.312 mg/mL. The results showed that all complexes exhibited promising antioxidant activities. Among them, $(PhCH_2NHCOCH_2)_2S{\cdot}DDQ$ compound had the least IC_{50} value of 6.725 mg/mL, indicating a potent scavenging property compared to other compounds. The molecular structures of charge-transfer complexes were investigated using hybrid density functional theory (B3LYP) and basis set 3-21G. We obtained geometrical structures' highest occupied molecular orbital (HOMO) and lowest unoccupied molecular orbital (LUMO) surfaces and energy gaps through geometric optimization. We also investigated the molecular shapes and contours of the prepared compounds through geometrical optimization and compared the HOMO energy of the CT compounds to investigate donor and acceptor properties.*

Keywords: *density functional theory; radical scavenging activity; organochalcogenide compound; quinone charge-transfer complexes; highest occupied molecular orbital*

■ INTRODUCTION

Charge-transfer complexes combine an electron donor with low ionization energy and an electron acceptor with high electronegativity. Some common examples of electron-donor compounds include amines, nitrogen–mixed bases, crown ethers, and organochalcogenides [1-8]. The spectra of these complexes are characterized by the appearance of a charge-transfer absorption band in the visible region resulting from electron transition between the highest occupied molecular orbital (HOMO) for a donor with the lowest unoccupied molecular orbital (LUMO) for the acceptor. This transition produces the characteristic intense color for these complexes, which can be used for quantitative drug estimation [9-10].

Charge-transfer complexes have become a subject of significant interest because of their unique physical

and chemical properties and potential application in various fields. One such area is the use of these complexes in 3rd generation solar cells, which are organic solar cells known for their efficient and cost-effective light absorbers [11-13]. Several physiologically and pharmacologically active charge-transfer complexes have been developed to treat various diseases. For example, piperazine and imidazole derivatives have shown promising anticancer activity [14-16]. Another exciting discovery involves the antimicrobial properties of the charge-transfer complexes formed between 3,5-dinitrosacylic acid and *o*-phenylenediamine intact DNA, demonstrating their antimicrobial activity, potentially valuable for developing various oncology drugs [17].

In recent decades, growing interest has been shown in synthesizing an essential class of compounds with diverse biological properties. The compounds are quinones that contain selenium or tellurium. The Se or Te atom is introduced into the quinones as an electrophile, using a suitable nucleophilic carbon such as a double bond, arylchalcogenyl halides or dichalcogenides. These compounds have been found to have a high potential as bioactive structures. We believe that further research into these compounds' synthesis and biological evaluation can lead to new biochemistry tools and new successes in drug development [18-21]. da Cruz and his co-workers [22] reported Se-containing quinone based on 1,2,3-triazoles, evaluating these compounds for antitumor activity *in vitro* using several human cancer cell lines. The results were promising as most compounds showed IC_{50} below 0.3 μM and were more active than doxorubicin and β-lapachone, a standard clinical agent for several types of cancers [21-22].

This study examined the charge-transfer complexes of organochalcogenide complexes as electron donors with 2,3-dichloro-5,6-dicyanobenzoquinones (DDQ), tetracyanoethane (TCNE), and 7,7',8,8'-tetracyanoquinodimethane (TCNQ) as electron acceptors. We prepared and characterized these complexes, evaluating their antioxidant activity experimentally using α,α-diphenyl-β-picrylhydrazyl (DPPH). To gain a deeper understanding of these compounds, we also conducted molecular structure and energy calculations using PM3 and density functional theory (DFT) at the B3LYP/3-21G level of theory.

■ EXPERIMENTAL SECTION

Materials

All diorganochalogenides were prepared under an argon atmosphere by the method preparation reported earlier [23]. Solvents were distilled prior to use and dried by conventional methods. Ascorbic acid, DPPH, TCNE, DDQ, and TCNQ with purity of 98% were purchased from Merck, Sigma-Aldrich.

Instrumentation

The FTIR spectra were measured on FTIR-8400S SHIMADZU-Japan, ^{1}H (400 MHz) and ^{13}C (100 MHz) NMR data were run on a Mercury-400 (Bruker Advance-NEO spectrometer) in DMSO-d_6 at ambient temperature. The UV-vis spectra were recorded on UV-1650PC: UV-visible spectrophotometer Shimadzu. The melting point of new charge-transfer complexes was determined on a Gallenkamp melting point apparatus. The antioxidant activity for all complexes was measured on the UV-vis spectrophotometer.

All theoretical calculations were conducted using computational methods implemented in the GAUSSIAN09 package [23]. Semi-empirical molecular orbital theory at the PM3 level was used to optimize the geometry optimization of the investigated compounds. The electronic properties of the compounds were analyzed by applying density functional theory at the B3LYP/3-21G theoretical level. The hybrid Becke-3-Lee-Yang-Parr exchange-correlation function (B3LYP) was used for DFT calculations [24].

Procedure

The following compounds, 2-chloro-*N*-phenylacetamide, 2-chloro-*N*-benzylacetamide, and 2-chloro-*N*-(*o*-tolylacetamide) were prepared according to the known chemistry literature [25].

*Preparation of bis-(*N*-(o-tolyl)acetamide)selenide*

Solution of $NaBH_4$ (0.236 g; 2.90 mmol) in 20 mL distal water was added to a suspended solution of Se powder (0.225 g; 6.10 mmol) in 20 mL of distal water

under an argon atmosphere with gentle heating. A vigorous reaction occurs with the release of hydrogen gases. A colorless solution of NaHSe was formed. A solution of 2-chloro-*N*-(*o*-tolylacetamide) (0.53 g; 2.90 mmol) in 30 mL ethanol was added to the above solution with stirring for 1 h. A violet solution was formed and filtered. As much as 100 mL of H_2O was added to this solution and extracted the resulting solution with three portions of chloroform. The solvent was evaporated to a minimum amount. A violet precipitate was collected, dried, and recrystallized from ethanol [25]. A violet solid was obtained (0.41 g) in 79% yield with melting point (m.p.) of 179 °C. The following compounds, bis(*N*-phenylacetamide)selenide (violet) (0.43 g) 82% yield, m.p. 204–205 °C and bis(*N*-benzylacetamide)selenide (dark yellow) (0.28 g) 60% yield, m.p.150 °C were also obtained.

*Preparation of bis(*N*-benzylacetamide)sulfide*

Solution of $Na_2S{\cdot}3H_2O$ (0.325 g; 246 mmol) in 10 mL distal water was added to a solution of 2-chloro-*N*-benzylacetamide (0.734 g; 4.92 mmol) in 30 mL of ethanol with gentle heat and stirring for about 1 h. A pale-yellow solution was formed, filtered, and added to 100 mL of distal water and the resulting solution was extracted with three portions of chloroform. The solvent was evaporated to a minimum amount. A pale-yellow solid was collected, dried, and recrystallized from ethanol. A pale-yellow solid was obtained (0.55 g) in 69% yield, m.p. 138–140 °C.

*Preparation of bis(*N*-benzylacetamide)telluride*

A mixture of 0.72 g (5.6 mmol) of Te powder and 0.364 g (5.6 mmol) of KCN in 25 mL of freshly distilled DMSO was stirred for 1 h at 100 °C under an Argon atmosphere. A pale-yellow solution of KTeCN formed, after cooling the mixture to laboratory temperature, solution of 1.68 g (11.2 mmol) of 2-chloro-*N*-benzylacetamide in 25 mL DMSO was added to it dropwise for 15 min and then stirred for 3 h at 100 °C [25]. The solution is filtered while it is hot, and then it is cooled and poured into 300 mL of cold distal water. A pale-yellow crystal was formed, filtered, washed several times with ethanol, and dried. A pale-yellow solid obtained in 70% yield, m.p. 105 °C [26].

*Preparation of bis(*N*-benzylacetamide)chalcogenide. DDQ charge-transfer complex; E = S, Se, and Te*

Solution of DDQ (0.227 g; 1 mmol) in 25 mL dry acetonitrile was added to the solution of bis(*N*-benzylacetamide)chalcogenide (0.222 g, 1 mmol) in 25 mL dry acetonitrile. The mixture was stirred with gentle heat for 2 h. A reddish solution was obtained directly, filtered, and evaporated to a minimum amount. Dark red crystals were collected, dried, and recrystallized from ethanol with 70–75% yield.

Bis(*N*-benzylacetamide)sulfide. DDQ CT complex (I): dark red color, 0.314 g (70%) yield, m.p. 120–123 °C.

(*N*-benzylacetamide)selenide. DDQ CT complex (II): dark red color, 0.43 g (75%) yield, m.p.105–107 °C.

Bis(*N*-benzylacetamide)telluride. DDQ CT complex (III): red color, 0.44 g (70%) yield, m.p. 167–170 °C.

The following compounds were prepared by the same procedure described [19].

Bis(*N*-(*o*-tolyl)acetamide)selenide. DDQ CT complex (IV); dark red solid, 0.439 g (73%) yield, m.p. 155–157°C.

Bis(*N*-phenylacetamide)selenide. DDQ CT complex (V); dark red solid, 0.39 g (68%) yield, m.p. 89–91 °C.

*Preparation of bis(*N*-benzylacetamide) E. TCNE CT complex, where E = S (VI), Se (VII)*

A mixture of 1 mmol tetracyanoethane in 25 mL dry acetonitrile and 1 mmol of $(PhCH_2NHCOCH_2)_2E$ in 25 mL dry acetonitrile was heated quietly with stirring for 2 h. The olive-green solution was obtained, filtered, and evaporated to a minimum amount. An olive green solid was collected, dried, and then recrystallized from ethanol. Olive-green solid was obtained in 75–80% yield.

*Preparation of bis(*N*-benzylacetamide)selenide. TCNQ CT complex (VIII)*

A mixture of 7,7'8,8'-tetracyanoquinodimethane (0.204 g; 1 mmol) in 25 mL dry acetonitrile and $(PhCH_2NHCOCH_2)_2S$ (0.328 g; 1 mmol) in 25 mL dry acetonitrile was heated gently with stirring for 2 h. A green solution was obtained, filtered and evaporated to a minimum amount. A dark green precipitate was collected, dried, and recrystallized from ethanol. A bright green solid was obtained 0.425 g (80%) yield, m.p. 96–

98 °C. The preparation of charge-transfer complexes has been carried out following reaction (Scheme 1).

Studying capacities for antioxidants

These complexes' antioxidant activity was evaluated experimentally using DPPH assay. The assay is a reliable analytical method for measuring various antioxidants' free radical scavenging capacities. The radical in the DPPH has a strong absorption maximum at 517 nm purple color. When this radical reacts with the antioxidant, the absorbance of DPPH decreases [27-28]. An aliquot of the test sample (1 mL) was added to 3 mL of 0.2 mM solution of DPPH prepared in methanol. Then, the reaction mixture was vortexed for 2 min and kept at room temperature for 30 min in the dark. The decreased absorbance was measured at 517 nm. The radical-scavenging activity was obtained using the Eq. (1);

$$\text{Scavenging activity (\%)} = \frac{A_C - A_t}{A_C} \times 100 \quad (1)$$

where A_C = Absorbance of blank, A_t = Absorbance of the sample. The required concentration mg/mL for inhibiting 50% of DPPH (IC_{50}) values was determined by linear regression (Table 1).

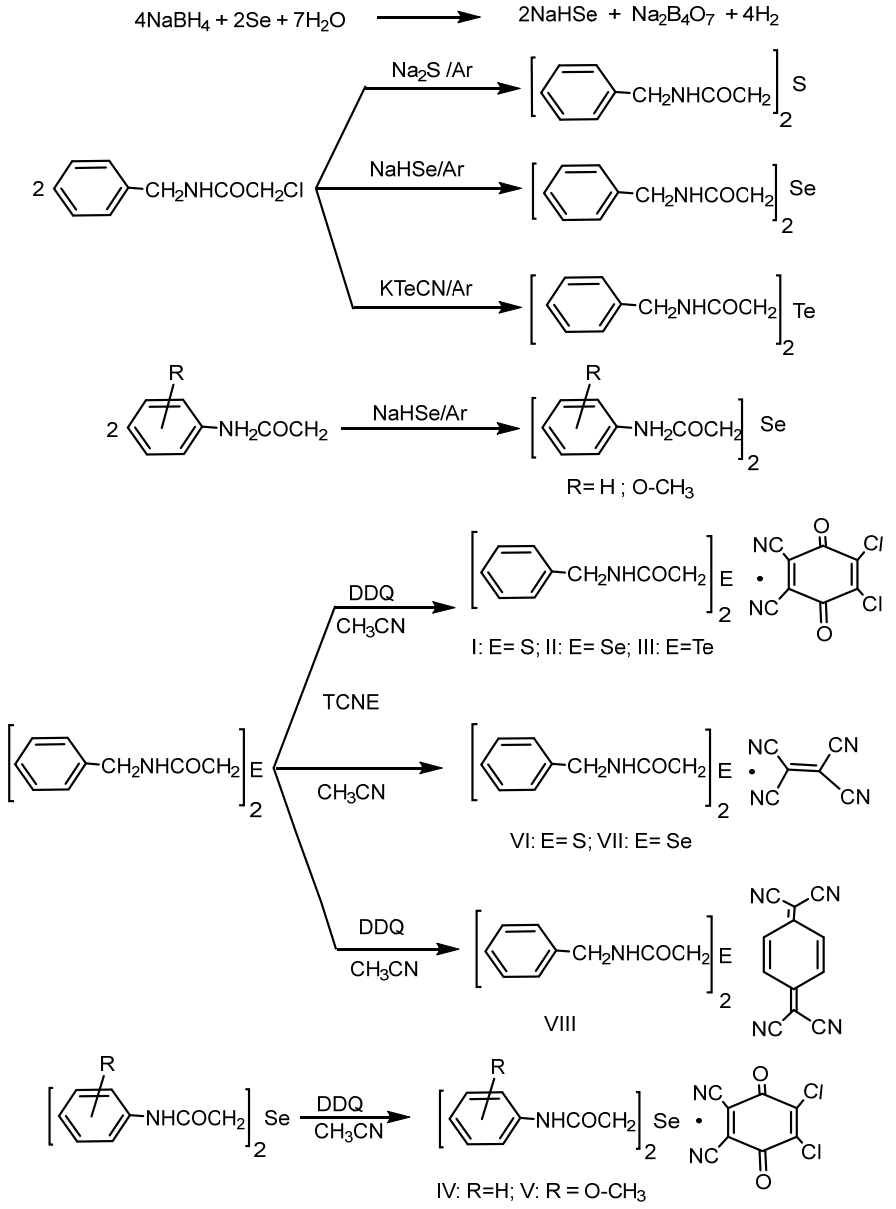

Scheme 1. Preparation of new charge-transfer complexes (I-VIII)

Table 1. Physical properties and UV-vis data for CT complexes

Comp.	Chemical structure	m.p. (°C)	Color	Yield (%)	λ_{max} (UV-vis, nm)
I	$(PhCH_2NHCOCH_2)_2S$·DDQ	120–122	Dark-red	70	217, 251, 354
II	$(PhCH_2NHCOCH_2)_2Se$·DDQ	105–107	Red	75	221, 233, 351, 391, 655
III	$(PhCH_2NHCOCH_2)_2Te$·DDQ	167–170	Red	70	215, 250, 351, 590
IV	$(PhNHCOCH_2)_2Se$·DDQ	155–157	Red	73	222, 256, 350, 474
V	$(o\text{-}CH_3PHNHCOCH_2)_2Se$·DDQ	89–91	Dark-red	68	214, 249, 364, 393
VI	$(PhCH_2NHCOCH_2)_2S$·TCNE	115–117	Green	75	214, 296, 396, 473, 647, 742
VII	$(PhCH_2NHCOCH_2)_2Se$·TCNE	192–195	Brown	80	215, 211, 276, 393
VIII	$(PhCH_2NHCOCH_2)_2S$·TCNQ	96–98	Bright-green	80	263, 311, 399, 474, 610, 735

■ RESULTS AND DISCUSSION

The reaction of $(PhNHCOCH_2)_2Se$, $(o\text{-}CH_3PhNHCOCH_2)_2Se$, and $(PhCH_2NHCOCH_2)_2E$, where (E = S, Se, and Te) as electron donors and quinones such as DDQ, TCNQ, and TCNE as electron acceptors in acetonitrile solution yield solid complexes 1:1 stoichiometry. Table 1 shows the structure and physical properties of new complexes. We focused on identifying functional groups in the quinones, specifically the C=O The and C≡N groups, by studying FTIR spectra of charge-transfer complexes. Additionally, we identified essential bands in organic chalcogenide such as N–H, C=O, C=C, C–E (E = S, Se, Te), C–H aliphatic, and C–H aromatic.

The FTIR spectra study of DDQ complexes I-V revealed some interesting findings. A slight shift was observed in the stretching vibration of the C≡N group, about ± 20 cm^{-1}. There was also a shift in the stretching vibration of the C=O group toward a large wavenumber with a change in the shape and some alteration in the intensity, indicating an interplay between the components of these complexes.

The TCNE charge-transfer complex VI exhibited a strong absorption band at 2,214 cm^{-1}, returning to the stretching vibration of the C≡N group. On the other hand, complex VII showed two bands at 2,210 and 2,075 cm^{-1}, returning to the stretching vibration of the C≡N group. Notably, the frequency of the C≡N group in free TCNE is 2,222 cm^{-1}. The TCNQ CT complex VIII exhibited a strong absorption band at 2,187 cm^{-1} due to the stretching vibration of the C≡N group in the $TCNQ^-$ ion radical. This mechanism indicates that the charge transfer from donor to acceptor is complete, and the TCNQ reduction to $TCNQ^-$ is complete [27-28]. Other unsymmetrical vibrations for C–H aromatic, C–H aliphatic, C=O and N–H for amide group, and C–E (E = S, Se and Te), were found at the expected region [24,29-30] as shown in Table 2 and Fig. S1-S8.

The study conducted in ethanol solvent at 200–800 nm examined the UV-vis spectra of charge-transfer complexes and their component. The results were included in Table 1 and Fig. S9. Organic molecules such as quinones have electron systems and possess strong absorption bands that appear in the UV region of the

Table 2. FTIR spectra data of prepared CT complexes

Comp.	N–H	C=O amide	C≡N	$C–H_{alip.}$	$C–H_{ar.}$	C=O DDQ	E–C E= S, Se or Te	C–Cl
I	3294	1647	2249	2924	3051	1801	698	748
II	3271	1643	2249	2924, 2866	3036	1740	613	775
III	3275	1643	2245	2854	3078	1710	498	732
IV	3255	1654	2222	2812	3070	1790	597	756
V	3240	1658	2245	2858	3032	1739	613	752
VI	3298	1647	2214	2924	3043	-	698	-
VII	3452	1647	2210, 2079			-	609	-
VIII	3298	1647	2187	2920	3039	-	698	-

spectrum due to the permitted transitions of type π-π* and n-π*. When these compounds bind with organochalcogenide compounds, a slight change occurs in the spectra of the new compounds. Additionally, new absorption bands emerge in the visible region, which can be attributed to charge transfer bands. DDQ charge-transfer complexes I-V show multi charged transfer bands at 350–364 nm, and new bands at 587, 474, and 393 nm, for CT complexes III, IV, and V, respectively. These bands are attributed to the electron transition from HOMO for the donor to LUMO for the acceptor [7,29-30]. Moreover, TCNE charge-transfer complex VI exhibited new bands at 396, 473, 647, and 742 nm, while CT VII showed a new band at 393 nm. TCNQ CT complex VIII exhibited new bands at 399, 474, 610, and 744 nm due to electron transfer from HOMO for the donor to LUMO for the acceptor [7,29-30].

^{1}H-NMR spectra of all new CT charge-transfer complexes in DMSO-d_6, and the results are tabulated in Table 3, Fig. S10-S16 and Scheme 2. The ^{1}H-NMR spectra displayed signals showing all the expected peaks. CT complexes I-VIII exhibited signals at 8.5–10.17 ppm that belonged to NH-amid proton [22,26,28]. The aromatic proton gives multiple signals in the range 6.69–7.59 ppm, while the aliphatic protons of CH_2E where (E = S, Se, and Te) displayed signals in the range 3.36–3.76 ppm [22,26,28]. However, we found that all complexes except IV and V exhibited signals in the range 4.27–4.49 ppm attributed to the proton of CH_2N [22,28,30].

^{13}C-NMR spectra of CT complexes were recorded in DMSO-d_6, and their data were summarized in Table 3 and Fig. S17-S22. Scheme 3 represents the numbering of carbon atoms of CT complexes**.** The ^{13}C-NMR spectra for new complexes agreed with their structures, further validating the characterization of these complexes. All CT complexes exhibit a low field signal in the range of 168.77–171.05 ppm attributed to the carbon of C=O (amide) group, they also exhibit low field signals of aromatic carbon atoms in the 119.55–139.73 ppm range. The DDQ CT complexes I-V displayed signals at 151, 114, and 102 ppm attributed to the carbon of C=O, C≡N, and C–CN, respectively [29,31-32]. Complexes I, VI, and VIII exhibited signals at 35.46–35.48 ppm belonging

Table 3. ^{1}H- and ^{13}C-NMR spectral data of selected CT complexes

Comp.	^{1}H-NMR (ppm), DMSO-d_6	^{13}C-NMR (ppm), DMSO-d_6
I	8.75(s)NH; 7.22–7.33(m)Ar–H; 4.33–4.37(s)H8,H9; 2.54(s)H6,H7	169.18 (C7); 114.18 (C≡N); 102.13 (C9); 151.29 (C10, C13); 139.67 (C11, C12); 42.78, 43.05 (C6); 35.48 (C8); 135.06, 129.96, 129.63, 128.77, 127.91, 127.68, 127.29 (Ar C)
II	8.56(s)NH; 7.22–7.45(m)Ar–H; 4.29(s)H8,H9; 3.39–3.38(s)H6,H7	170.32 (C7); 114.19 (C≡N); 102.14 (C9); 151.31 (C10, C13); 139.73 (C11, C12); 42.77 (C6), 26.07 (C8); 129.66, 128.77, 127.77, 127.66, 127.28 (Ar C)
III	8.56(s)NH; 7.22–7.46(m)Ar–H; 4.26–4.31(s)H8,H9; 3.52(s)H6,H7	166.57, 164.84 (C7); 112.57 (C≡N); 100.50 (C9); 149.69 (C10, C13); 137.87, 137.68 (C11, C12), 41.50, 41.33 (C6); 37.95, 37.74 (C8); 128.04, 127.17, 127.03, 126.35, 126.15, 126.05, 125.78, 125.75 (Ar C)
IV	10.17(s)NH; 7.26–7.32(m); 7.03–7.06 Ar–H; 3.52(s)H6,H7	169.15 (C7); 114.23 (C≡N); 102.10 (C9; C14); 151.31, 145.11 (C10, C13); 139.51 (C11, C12); 34.86 (C6); 27.40, 27.08 (C8); 136.74, 129.65, 129.23, 123.82, 119.55, 118.55 (Ar C)
V	9.68(s)NH; 7.01–7.32(m)Ar–H; 3.40(s)H6,H7; 2.16(S)H(CH_3)	169.29, 168.77 (C7); 114.19 (C≡N); 102.13 (C9, C14) 102.13; 151.31 (C10, C13); 136.59 (C11, C12); 26.73 (C8); 18.35 (CH_3); 131.82, 130.79, 129.64, 126.43, 126.19, 125.62, 125.03 (Ar C)
VI	8.58(s)NH; 7.21–7.34(M)Ar–H; 4.33(s)H8,H9; 3.32(s)H6,H7	169.17 (C7); 42.77 (C6); 35.47 (C8); 139.68 (C9, C10); 58.26, 128.78, 128.54,127.69, 127.30 (Ar C)
VII	8.46(s)NH; 6.79–6.9(m)Ar–H; 4.43(s)H8,H9; 3.83(s)H6,H7	171.05 (C7); 45.39 (C6); 23.17 (C8); 132.12, 127.21, 119.22 (Ar C); 104.9 (C≡N); 96.22 (C9, C10)
VIII	8.6(s)NH; 6.9–7.43(m)Ar–H; 4.31(s)H8,H9; 3.21(s)H6,H7	169.33 (C7); 42.76 (C6); 35.46 (C8); 128.83, 127.72, 127.33 (Ar C); 112.58 (C≡N); 139.73 (C11, C14); 96.55 (C10, C15); 120.93 (C10-13)

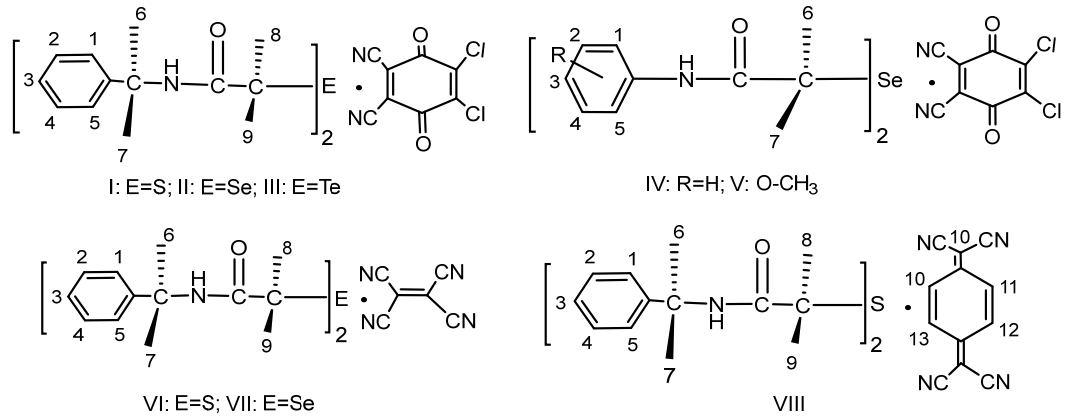

Scheme 2. Expected structure for new CT complexes

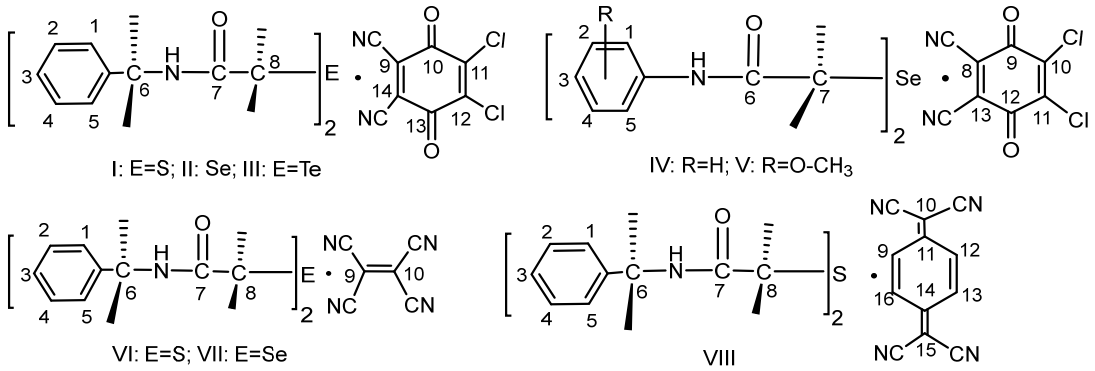

Scheme 3. The numbering of carbon atoms of CT complexes

to a carbon of CH_2–S, while complexes II, IV, V, and VI gave a signal in the range of 23.17–27.40 ppm, with the carbon of CH_2–Te exhibited at 37.95 ppm [7,30,33].

Antioxidant Study

Antioxidants are essential molecules capable of preventing or slowing down the oxidation of free radicals through various mechanisms. One method to measure the antioxidant potential of compounds or specific extracts is through the DPPH free radical scavenging methods. This method reduces the odd electron on the N atom in the stable free radical DPPH by receiving a H atom from the antioxidant to the corresponding hydrazine, as shown in Scheme 4.

DPPH free radical was used at a concentration of 10–0.312 mg/mL to investigate the antioxidant activity of new complexes. All CT complexes showed encouraging antioxidant activities. The compounds' effectiveness can be arranged as follows:

I > IV > VIII > III > VI > II > V

$(PhCH_2NHCOCH_2)_2Se$·DDQ compound (I) has the lowest IC_{50} value of 6.72 mg/mL compared to other CT complexes, as shown in Table 4. The lower the IC_{50} value, the greater the oxidant potency in a compound.

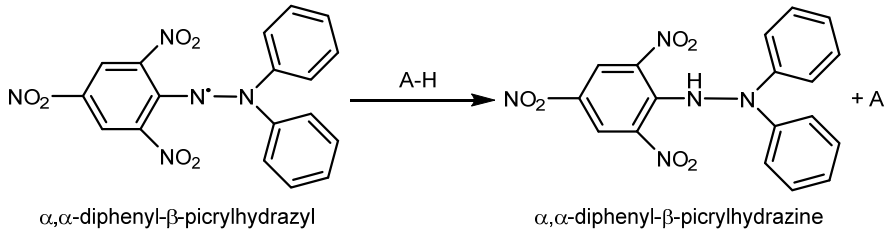

Scheme 4. Free radical (DPPH) and its reduction by an antioxidant A–H compound

Table 4. The IC_{50} for new CT complexes

Compound	IC_{50} (mg/mL)
I	6.72
II	36.87
III	10.67
IV	8.35
V	42.7
VI	21.8
VIII	10.4

Computational Study

We used the computational methods in the GAUSSIAN09 package to perform all theoretical calculations in this work [22]. The theoretical planes B3LYP/3-21G* and B3LYP/6-31G* were used to obtain the optimized geometries of the compounds. However, we only used the B3LYP/3-21G* method for frequencies and could not perform B3LYP/3-21G* frequencies due to computational constraints [22-23]. Our study found that the DFT-B3LYP method accurately predicted the experimental parameters [34]. In recent years, DFT-based theoretical approaches have emerged as a viable alternative to traditional *ab initio* methods for investigating the structure and reactivity of chemical systems. Therefore, we used this method to optimize the geometry of stationary points using the Berny analytical gradient optimization method.

HOMO and LUMO energies are electronic states that denote a specific location where electrons with quantized energy and molecular orbitals are linearly coupled to atomic orbitals. The difference between the HOMOs gives the energy band gap (E_g) as a crucial property in solids because it can predict whether it is a conductor, insulator, or semiconductor. The energy band represents the energy difference between lower virtual and higher full energy levels [35]. Table 5 displays the comparison of HOMO and LUMO energies. All the prepared compounds' E_{gap} configurations indicated that the E_{gap} was highest in the VII compound and lowest in the VI compound [7,28-29] as shown in Table 5 and Fig. S23-S30.

VII > III > VIII > II > I > V> IV > VI

Electronegativity (χ) is a captivating concept, measuring an atom's tendency to attract a pair of shared electrons to itself. On the other hand, relative rate constants measure the electrophilicity of different electrophilic reagents as they react with a common substrate (usually involving an attack on a carbon atom). In Table 6, the electronegativity of VII is greater than that of the rest compounds, as shown as follows:

VII > VIII > VI > III > I > II > IV > V

Compound VII has the highest electrophilicity (ω), while compound VI has the least ω. As this arrangement:

VI > IV > V > VIII > VII >I > II > III

Ionization potential (I) explains this trend, which measures the bonding force between electrons and atoms. Ionization potential indicates the energy required to remove one electron from a neutral atom in a gaseous state. On the other hand, electron affinity is the energy released when an atom gains an electron. It corresponds to the energy required to remove one electron from a negative ion. According to Koopman's theorem, the ionization potential and electron affinity depend on the energies of the valence and conduction bands [23], Table 6 shows the values of ionization potential and electron affinity for compounds I-VIII, according to Koopman's

Table 5. Showing the electronic structure of a prepared compound

Comp.	HOMO	LUMO	E_{Gap}
I	−4.46516	−3.7305	0.7347
II	−4.5223	−3.6706	0.8517
III	−4.60937	−3.6244	0.985
IV	−4.26653	−3.891	0.3755
V	−4.32367	−3.8284	0.4952
VI	−4.33183	−4.0298	0.302
VII	−5.83655	−4.6828	1.1537
VIII	−5.70594	−4.7835	0.9224

Table 6. Conformational parameters (eV) of all optimized structures

Comp.	(I)	(A)	(χ)	(η)	(σ)	(ω)
I	4.4652	3.7305	4.098	0.367	2.722	22.86
II	4.5223	3.6706	4.096	0.426	2.348	19.70
III	4.6094	3.6244	4.117	0.493	2.03	17.21
IV	4.2665	3.891	4.079	0.188	5.326	44.30
V	4.3237	3.8284	4.076	0.248	4.039	33.55
VI	4.3318	4.0298	4.181	0.151	6.622	57.87
VII	5.8365	4.6828	5.26	0.577	1.734	23.98
VIII	5.7059	4.7835	5.245	0.461	2.168	29.82

theorem. From the table, we can see the arrangement of the prepared compounds according to the decrease in ionization potential [35-36]:

VII > VIII > III > II > I > VI > V > IV

It is beneficial that less energy is required for electrons to escape from the surface [34-35]. The electron affinity (A) decreased as follows:

VIII > VII > VI > IV > V > I > II > III

This principle describes the behavior of molecules or atoms compared to the acids and bases in chemistry. Notably, bases represent donors but acids stand for acceptors [34,36-38]. When comparing compounds I–VIII, the hardness (η) of VII is greater than that of the rest of the prepared compounds, and thus VII behaves as a hard base. In contrast, VI is a soft base, as its softness is greater than VII's [7,35,37-39].

VII > III > VIII > II > I > V > IV > VI

According to Table 6, the behavior of the prepared compounds can be classified as donor or acceptor [7,35,37-39].

VI > IV > V > I > II > VIII > III > VII

■ CONCLUSION

This study prepared a new series of CT complexes based on the reaction of organochalcogenides as electron donors with DDQ, TCNE, and TCNQ as electron acceptors in acetonitrile. Various spectroscopic techniques characterize all prepared complexes, and all complexes showed promising antioxidant activity using DPPH free radicals at different concentrations. Complex I exhibited the most potent scavenging property compared to other compounds compared to other charge-transfer compounds with the least IC_{50} value of 6.725 mg/mL. Our theoretical studies found that the DFT is a powerful method, and the B3LYP functional is an efficient function suitable for studying the electronic properties of these structures. We used DFT to analyze the prepared compounds' geometrical optimization and electronic properties using the B3LYP functional. The geometry and donor-acceptor system for all energies indicates that this structure is more stable. We found that the donor-acceptor system is more reactive than the donor-acceptor system, with a larger average polarization ratio. These results help select the type of bridge that interacts with the donor and acceptor and calculate the physical properties of the donor-bridge-acceptor system.

■ ACKNOWLEDGMENTS

The authors express their gratitude to I.A. Al-Timimi (Department of Chemistry, University of Basrah) for her assistance in performing the UV-vis analysis.

■ CONFLICT OF INTEREST

The authors declare no conflict of interest.

■ AUTHOR CONTRIBUTIONS

Conceptualization and experimental design: Attared Fadhel Hassan, Nahed Hazim Al-Haidery and Shaker Abdel Salem Al-Jadaan; antioxidant study: Sabah Abbas Malik; computational study: Nuha Hussain Al-Saadawy; experimental work: Attared Fadhel Hassan, Nahed Hazim Al-Haidery and Suhad Rajab Kareem; data analysis, writing-original draft preparation: Attared Fadhel Hassan and Nuha Hussain Al-Saadawy. All authors have read and agreed to a published version of the manuscript.

■ REFERENCES

[1] AlQaradawi, S.Y., Mostafa, A., and Bengali, A.A., 2016, Charge-transfer complexes formed in the reaction of 2-amino-4-ethylpyridine with π-electron acceptors, *J. Mol. Struct.*, 1106, 10–18.

[2] Wu, L., Wu, F., Sun, Q., Shi, J., Xie, A., Zhu, X., and Dong, W., 2021, A TTF–TCNQ complex: An organic charge-transfer system with extraordinary electromagnetic response behavior, *J. Mater. Chem. C*, 9 (9), 3319–3323.

[3] Darwish, I.A., Khalil, N.Y., Asaif, N.A., Herqash, R.N., Sayed, A.Y., and Abdel-Rahman, H.M., 2021, Charge-transfer complex of Linifanib with 2,3-dichloro-3,5-dicyano-1,4-benzoquinone: Synthesis, spectroscopic characterization, computational molecular modelling and application in the development of novel 96-microwell spectrophotometric assay, *Drug Des., Dev. Ther.*, 15, 1167–1180.

[4] Adam, A.M.A., and Refat, M.S., 2021, A comparison of charge-transfer complexes of iodine with some antibiotics formed through two different approaches (liquid-liquid vs solid-solid), *J. Mol. Liq.*, 329, 115560.

[5] Khan, I.M., Alam, K., and Alam, M.J., 2020, Exploring charge transfer dynamics and Photocatalytic behavior of designed donor-acceptor complex: Characterization, spectrophotometric and theoretical studies (DFT/TD-DFT), *J. Mol. Liq.*, 310, 113213.

[6] Kato, Y., Matsumoto, H., and Mori, T., 2021, Absence of HOMO/LUMO transition in charge-transfer complexes thienoacenes, *J. Phys. Chem., A*, 125 (1), 146–153.

[7] Mohammed, H.M., and Al-Saadawy, N.H., 2022, Synthesis, characterization, and theoretical study of novel charge-transfer complexes derived from 3,4-selenadiazobebzophenone, *Indones. J. Chem.*, 22 (6), 1663–1672.

[8] Al-Rubaie, A.Z., and Al-Masoudi, E.A., 1990, Charge-transfer complexes of 5,6-dimethyl,1,3-dihydro-2-telluraindene, with quinones, *Polyhedron*, 9 (6), 847–849.

[9] Yousef, T.A., Ezzeldin, E., Abdel-Aziz, H.A., Al-Agamy, M.H., and Mostafa, G.A.E., 2020, Charge transfer complex of neostigmine with 2,3-dichloro-5,6-dicyano-1,4-benzoquinone: Synthesis, spectroscopic characterization, antimicrobial activity, and theoretical study, *Drug Des., Dev. Ther.*, 14, 4115–4129.

[10] Shehab, O.R., AlRabiah, H., Abdel-Aziz, H.A., and Mostafa, G.A.E., 2018, Charge-transfer complexes of cefpodoxime proxetil with chloranilic acid and 2,3-dichloro-5,6-dicyano-1,4-benzoquinone: Experimental and theoretical studies, *J. Mol. Liq.*, 257, 42–51.

[11] Khan, I.M., and Ahmad, A., 2010, Synthesis, spectral and thermal studies of newly Hydrogen bonded charge transfer complex of *o*-phenylenediamine with π acceptor picric acid, *Spectrochim. Acta, Part A*, 77 (2), 437–441.

[12] Lee, S., Hong, J., Jung, S.K., Ku, K., Kwon, G., Seong, W.M., Kim, H., Yoon, G., Kang, I., Hong, K., Jang, H.W., and Kang, K., 2019, Charge-transfer complexes for high-power organic rechargeable batteries, *Energy Storage Mater.*, 20, 462–469.

[13] Divyasree, M.C., Vasudevan, K., Abdul Basith, K.K., Jayakrishnan, P., and Ramesan, M.T., 2018, Third-order nano linear optical properties phenothiazine-iodine charge transfer complexes in different proportions, *Opt. Laser Technol.*, 105, 94–101.

[14] Gaballa, A.S., and Amin, A.S., 2015, Preparation, spectroscopic and antibacterial studies on charge-transfer complexes of 2-hydroxypyridine with picric acid and 7,7′,8,8′-tetracyano-*p*-quinodimethane, *Spectrochim. Acta, Part A*, 145, 302–312.

[15] Alam, K., and Khan, I.M., 2018, Crystallographic, dynamic and Hirshfeld surface studies of charge transfer complex of imidazole as a donor with 3,5-dinitrobenzoic acid as an acceptor: Determination of various physical parameters, *Org. Electron.*, 63, 7–22.

[16] Khan, I.M., Ahmad, A., and Oves, M., 2010, Synthesis, characterization, spectrophotometric, structural and antimicrobial studies of new charge transfer complexes of *p*-pheylenediamine with π acceptor picric acid, *Spectrochim. Acta, Part A*, 77 (5), 1059–1064.

[17] Basha, M.T., Alganmi, R.M., Soliman, S.M., Abdel-Rahman, L.H., Shehata, M.R., and Aharby, W.J., 2022, Synthesis, spectroscopic characterization, biological activity, DNA-binding investigation combined with DFT studies of new proton-transfer complexes of 2,4-diaminopyrimidine with 2,6-dichloro-4-nitrophenol and 3,5-dinitrosalcylic acid, *J. Mol. Liq.*, 350, 118508.

[18] Cordeiro, P.S., Chipoline, I.C., Ribeiro, R.C.B., Pinho, D.R., Ferreira, V.F., da Silva, F.C., Forezi, L.S.M., and Nascimento, V., 2022, Seleno-and telluro functionalization of quinones: Molecules with relevant biological application, *J. Braz. Chem. Soc.*, 33 (2), 111–127.

[19] Fu, X., Li, S., Jing, F., Wang, X., Li, B., Zhao, J., Liu, Y., and Chen, B., 2016, Synthesis and biological evaluation of novel 1,2,4-thiadiazole derivatives incorporating benzisoselenazolone scaffold as

potential antitumor agents, *Med. Chem.*, 12 (7), 631–639.

[20] Shabaan, S., Ba, L.A., Abbas, M., Burkholz, T., Denkert, A., Gohr, A., Wessjohann, L.A., Sasse, F., Weber, W., and Jacob C., 2009, Multicomponent reactions for synthesis of multifunctional agents with activity against cancer, *Chem. Commun.*, 4702–4704.

[21] Arora, E., 2023, Synthetic methodologies and applications of chalcogen (S, Se, Te) ionic liquids: A review, *Phosphorus Sulfur Silicon Relat. Elem.*, In Press, Corrected Proof.

[22] da Cruz, E.H.G., Silvers, M.A., Jardim, G.A.M., Resende, J.M., Cavalcanti, B.C., Bomfim, I.S., Pessoa, C., de Simone, C.A., Botteselle, G.V., Braga, A.L., Nair, D.K., Namboothiri, I.N.N., Boothman, D.A., and da Silva Júnior, E.N., 2016, Synthesis and antitumor activity of selenium-containing quinone-based triazoles possessing two redox centres, and their mechanistic insights, *Eur. J. Med. Chem.*, 122, 1–16.

[23] Cao, L.M., Hu, C.G., Li, H.H., Huang, H.B., Ding, L.W., Zhang, J., and Chen, X.M., 2022, Molecule-enhanced electrocatalysis of sustainable oxygen evolution using organoselenium functionalized metal–organic nanosheets, *J. Am. Chem. Soc.*, 145 (2), 1144–1154.

[24] Taha, D.K., Israa, H.H., and Rashid, H.J., 2021, Theoretical properties of Ni_2Ti alloys studied: By Gaussian 09 program, *J. Phys.: Conf. Ser.*, 1818 (1), 012054.

[25] Hassan, A.F., Abdulwahid, A.T., Al-Luaibi, M.Y., and Aljadaan, S.N., 2020, Synthesis, characterization and thermal study of some new organochalcogenide compounds containing arylamide group, *Egypt. J. Chem.*, 64 (9), 5009–5015.

[26] Ahmed, W.M., Al-Saadawy, N.H., and Abowd, M.I., 2021, Synthesis and characterization of a new organoselenium and tellurium compounds depending on 9-chloro-10-dihydroanthracene, *Ann. Rom. Soc. Cell Biol.*, 25 (4), 11035–11043.

[27] Shakibaie, M., Adeli-Sardou, M., Mohammadi-Khorsand, T., Zeydabadi-Nejad, M., Amirafzali, E., Amirpour-Rostami, S., Ameri, A., and Forootanfar, H., 2017, Antimicrobial and antioxidant activity of the biologically synthesized tellurium nanorods; A preliminary *in vitro* study, *Iran. J. Biotechnol.*, 15 (4), 268–276.

[28] Forootanfar, H., Adeli-Sardou, M., Nikhoo, M., Mehrabani, M., Amir-Heidari, B., Shahverdi, A.R., and Shakibaie, M., 2014, Antioxidant and cytotoxic effect of biologically synthesized selenium nanoparticles in comparison to selenium dioxide, *J. Trace Elem. Med. Biol.*, 28 (1), 75–79.

[29] Kitzmann, W.R., and Heinze, K., 2023, Charge-transfer and spin-flip states: Thriving as complements, *Angew. Chem. Int. Ed.*, 62 (15), e202213207.

[30] Juliá, F., 2022, Ligand-to-metal charge transfer (LMCTt) photochemistry at 3d-metal complexes: An emerging tool for sustainable organic synthesis, *ChemCatChem*, 14 (19), e202200916.

[31] Khalib, A.A.K., Al-Hazam, H.A.J., and Hassan, A.F., 2022, Inhibition of carbon steel corrosion by some new organic 2-hydroselenoacetamide derivatives in HCl medium, *Indones. J. Chem.*, 22 (5), 1269–1281.

[32] Hassan, A.F., Radhy, H.A., and Essa, A.H., 2009, Synthesis of charge-transfer complexes for 5,6-dimethyl-2,1,3-benzoselenadiazole, *J. Sci. Res.*, 1 (3), 569–575.

[33] Mostafa, G.A.E., Yousef, T.A., Gaballah, S.T., Homoda, A.M., Al-Salahi, R., Aljohar, H.I., and AlRabiah, H., 2022, Quinine charge transfer complexes with 2,3-dichloro-5,6-dicyano-benzoquinodimethane: Spectroscopic characterization and theoretical study, *Appl. Sci.*, 12, 987.

[34] AdilAjeel, A., and Al-Saadawy, N.H., 2021, Preparation and identification of new organoselenium compounds based on *N*-phenyl-2-selenocyanatoacetamide, *Nat. Volatiles Essent. Oils*, 8, 8090–8111.

[35] Chand, S., Tyagi, M., Tyagi, P., Chandra, S., and Sharma, D., 2019, Synthesis, characterization, DFT of novel, symmetrical, N/O-donor tetradentate Schiff's base, its Co(II), Ni(II), Cu(II), Zn(II) complexes and their *in-vitro* human pathogenic

antibacterial activity, *Egypt. J. Chem.*, 62 (2), 291–310.
[36] Zhao, J., Song, P., Feng, L., Wang, X., and Tang, Z., 2023, Theoretical insights into atomic-electronegativity-regulated ESIPT behavior for B-bph-fla-OH fluorophore, *J. Mol. Liq.*, 380, 121763.
[37] Yang, D., Yang, W., Tian, Y., and Lv, J., 2023, Unveiling the effects of atomic electronegativity on ESIPT behaviors for FQ-OH system: A theoretical study, *Spectrochim. Acta, Part A*, 286, 122007.
[38] Zhao, J., Jin, B., and Tang, Z., 2023, Theoretical revealing regulated ESIPT behaviors by atomic electronegativity for quercetin fluorophore, *Chem. Phys. Lett.*, 810, 140194.
[39] Yin, F., and Fang, H., 2022, Unveiling the effects of atomic electronegativity on the ESIPT mechanism and luminescence property of new coumarin benzothiazole fluorophore: A TD-DFT exploration, *Spectrochim. Acta, Part A*, 275, 121118.